PNAS
www.pnas.org

Supplementary Information for

Predator-informed looming stimulus experiments reveal how large filter feeding whales capture highly maneuverable forage fish

David E. Cade
Nicholas Carey
Paolo Domenici
Jean Potvin
Jeremy A. Goldbogen

Corresponding author:
Email: davecade@stanford.edu

This PDF file includes:

Other supplementary materials for this manuscript include the following:

www.pnas.org/cgi/doi/10.1073/pnas.1911099116

Supplementary Information Text

List of abbreviations

α:	The apparent angle of an approaching predator or stimulus subtended on the retina of the prey
AF:	Anchovy-feeding
AMO:	Apparent Mouth Opening
CATS:	Customized Animal Tracking Solutions
dα/dt:	The change in the size of the looming stimulus over time (aka the loom rate)
E_{in}:	Energy from food (input)
E_{out}:	Energy expended (output)
HF:	High frequency
IACUC:	Institutional Animal Care and Use Committee
KF:	Krill-feeding
LT:	Looming Threshold
LT_{exp}:	experimentally determined Looming Threshold of response (in rad s^{-1})
MC:	Mouth Closing
MO:	Mouth Opening
SD:	Standard deviation
SE:	Surplus efficiency
SI:	Supplemental Information
SoCal:	Southern California study region
UAV:	Unoccupied Aerial Vehicle
U_{pred}:	Speed (of a predator)

Materials and Methods

This work used a combination of field data, laboratory experiments and modeling to describe the predator/prey interactions of humpback whales and anchovies. We first used mean published data on anchovy-feeding (AF) and krill-feeding (KF) humpback whales from (2) to parameterize laboratory looming threshold experiments with individual anchovies in the lab (see below). After determining the timing of anchovy escape responses to virtually approaching whales, we used new field data and the results of the laboratory experiments to test how predator speed, the timing of engulfment in relation to acceleration, and the timing of mouth opening in relation to a prey school affected how many fish a humpback whale could catch, and how much energy it spent doing so. We divided humpback whale attacks into two categories: Type 1 was the mean of new data from fast attacking whales tagged in Southern California (SoCal) feeding on mobile patches of anchovies ~1-2 m across; Type 2 was the mean of a previously published, slow-attacking whale from Monterey Bay, California (2) feeding on an anchovy school several times larger than its own size.

Field data collection and analysis

The humpback whale approach speeds used to create the looming stimuli in the lab experiments were averaged speed profiles derived from the krill-feeding and anchovy-

feeding humpback whales in (2). Data from additional humpback whales used for escape simulations were collected in August 2017 near Santa Barbara, California using suction-cup attached video and movement sensing tags from Customized Animal Tracking Solutions (CATS) (2, 3). All tags were deployed from a 6 m rigid-hull inflatable boat using a 6 m pole (Fig. 1a) under National Marine Fisheries Service permits 16111 as well as institutional IACUC protocols. Accelerometers were sampled at 400 Hz, magnetometers and gyroscopes at 50 Hz and, pressure, light, temperature and GPS at 10 Hz. All data were decimated to 10 Hz, tag orientation on the animal was corrected for, and animal orientation was calculated using custom-written Matlab scripts (following 2, 4). Animal speed for all deployments was determined using the amplitude of tag vibrations (5).

Engulfment timing from on-animal videos of humpback whales attacking anchovies was determined from the first indication of head rise and the last indication of the head falling (2). School dispersion happened over a range of times and parts of the targeted schools were blocked from view by the whale's body. Thus, it was not possible to determine the timing of the first fish to flee, however a time of school dispersion was estimated from the first time at least 50% of the visible school was observed to be scattering.

Fish Husbandry

All anchovies (*Engraulis mordax*) came from a stock of approximately 400 individuals kept at Hopkins Marine Station, Pacific Grove, CA, USA, in a 3200 L circular tank (2.5 m diameter, 0.65 m deep) supplied with flow-through seawater at 20 L min^{-1}, and fed 4 times daily on a mix of freeze-dried krill and commercial fish feed (2 mm sinking pellets, Skretting, UT, USA), at 0.4 g per individual per day. Fish constantly circled this tank as one large school. This work was conducted under Stanford IACUC permit no. 28859 for working on fish.

Creation of attack scenarios and looming animations

Three different models (Movie S3, Code S1) were played back to anchovies: 1) a constant speed simulation typically used in looming threshold experiments (6-10), 2) a model based on the mean anchovy-feeding (AF) data from (2) and 3) a model based on the mean krill-feeding (KF) data from (2). The constant speed scenario was a 2.8 s looming stimulus animation modelled on a disc the size of an average humpback whale's girth (2.65 m diameter) approaching at a constant speed of 5 m s^{-1} (Movie S3). AF and KF models were formulated using observed speed and engulfment parameters (timing of mouth opening and maximum gape) as well as size inputs from an average sized whale of 10.5 m length, with lower jaw max extension to 50°, upper jaw max extension to 30°, and with other characteristics including jaw length (2.25 m), whale diameter (2.51 m) and max girth location (4.41 m from the rostrum) allometrically or proportionally determined from the input length (11). Code S1 was used to create the looming animations using these parameters at a refresh rate of 60 Hz, such that the hypothesised viewing conditions from the prey perspective would be accurately recreated during playback. The stimulus is assumed to be perceived by the anchovies as a smooth animation of an approaching object, since the 60 Hz refresh rate is likely above that of the flicker fusion frequency of visual system of the prey. Although values of flicker fusion frequency of anchovies are not available, that of most fish species are below 60 Hz (12, 13).

For each frame of the model, the visual angle (α, Fig. 1) of the whale from the target's viewpoint was calculated as well as the rate of change of α (dα/dt). Up to a certain point in the model the apparent α of the whale is determined by its maximum girth and its distance from the target. However, the jaws of a humpback whale can extend beyond the whale's girth (in the 10.5 m whale length example the jaws can be up to 2.86 m wide). Thus, at the point when the combined viewing angle of the opening upper and lower jaws exceeds that of the maximum girth, α is determined by the combined angle and distance of the upper and lower jaws. For simulations of catch percentage (see below), if the whale approaches close to a fish school before opening its jaws, there can also be an intermediate point at which α is determined by a part of the whale anterior to the maximum girth. This scenario arises because although humpback whales are fusiform in shape they are not perfectly conical. In both the AF & KF playback experiments, however, the stimulus was constructed such that a fish located 16 cm from the screen would be reached by the virtual whale at the point when its jaws would be at maximum gape, and this point is far enough from the whale that α is not substantially different from the α of maximum girth until after the jaws dominate α (Fig. 1, S7a). Thus, for simplification in interpreting the playback experiment results, this intermediate α was excluded from the stimulus during playbacks but included in later simulations of catch percentage that involved schools of responding fish.

Escape Response Experiments

Escape response experiments were conducted in a 144 L glass tank (0.3 m wide, 1.2 m long, 0.4 m water depth), illuminated with LED strip lighting around its top edge. Three sides were covered with white board, with one long side left uncovered to allow side-view filming (Fig. 1). The entire tank and filming area were screened off from view using tarpaulins. A 17" LCD monitor was placed along the long side of the tank directly against the glass, visible through a cut-out in the screening. Two Edgertronic SC1 cameras (Sanstreak Corp, San Jose, California USA) were mounted in orthogonal positions, one directly above the midpoint of the width of the tank, the other at the side, positioned to capture part of the tank including the playback screen (Fig. 1). One camera was slaved to the other so that when triggered, 6 seconds of simultaneous footage preceding the trigger time was captured from both cameras at 250 Hz. Calibration videos were recorded before any experiments were conducted.

Fish were moved in groups of 7-9 individuals from the holding tank to the filming tank using a mesh net and observed for several minutes from a concealed position. Individuals which showed ongoing erratic behavior (e.g. swimming against the glass, darting) were removed to minimize disturbance to the remaining fish and placed in a separate holding tank. These individuals were not reused for any experiments. This left individuals which appeared to be in a calmer state (though with apparent heightened awareness) which typically swam up and down the length of the tank. These remaining fish were left for approximately 10 minutes further before being exposed to the looming animations. During this time, occasional videos were recorded of the fish turning spontaneously, and kinematic criteria to distinguish escape responses from spontaneous turns were independently established (see below). Occasionally fish manifested erratic behavior later in the trials, disturbing the other fish, and these individuals were removed as

above. As a result, responses were captured with different total numbers of fish in the tank, including some with only a single fish remaining.

Like other pelagic fish, anchovies are continuous swimmers and therefore looming animation video playback (which was between 3 and 4 s depending on the scenario) had to be timed so that in the course of their swimming patterns up and down the tank, a particular fish would view the animation in its entirety and also be close to the midpoint of the width of the tank, at the assumed viewing distance of 16 cm from the screen. Fish that were determined post-hoc to be more than 16 ± 3 cm from the screen at the time of response were excluded from analysis to maintain comparable apparent approach speeds. Fish were observed through a gap in the screening and the looming animations triggered manually when it was judged the swimming pattern of a particular fish might meet these criteria. Until playback was triggered, the screen displayed the initial frame of the animation, which in all scenarios consisted of a 3 cm black circle. This starting size was chosen so as to be relatively unobtrusive but also to make the animation a manageable duration so that playback could be timed correctly. When the animation was triggered, a live view from the camera was viewed on a laptop. If it was judged an escape response occurred, the video was saved. To maximise the chances of obtaining successful responses, and because correct timing of the animation to the fish position was extremely difficult, several playbacks of the animation were conducted for each group.

Escape response video processing

In total, approximately 350 anchovies were moved to the experimental tank for exposure to the looming animations. Over the three attack scenarios, a total of 130 anchovies demonstrated sharp lateral turns away from the screen coincident with animation playback. Of these recordings, 90 met the quality conditions for digitization. Of these, 30 (10 for the constant speed, 11 for AF and 9 for KF) met the criteria of being responses by unique individuals within ± 3 cm of the assumed viewing distance of 16 cm.

Overhead videos of potential escape responses were reviewed to determine the frame at which the response occurred, defined as the frame at which the specimen's turn away from the stimulus was initiated (Fig 1). The matching frame from the side-view video was used to identify the frame of the animation (and thus stage of the hypothetical attack) at which the response was initiated, via the frame indicator numbers visible on the playback screen (Movie S3). Overhead videos (Movie S5) were manually digitised using the DLTdv5 library for Matlab (14) to provide spatial XY coordinates. All further data processing was conducted in R. The XY coordinates were used to determine the turning rate of the fish away from the stimulus in $^\circ\ s^{-1}$. Turning rate was defined as the angular velocity of the anterior part of the body (represented by a line joining two digitised point, i.e. the tip of the head and a point at 20% of the fish's body length), between its position before and at the end of the turn (15). Twenty spontaneous turns were also digitized and turning rate of these likewise determined. The mean turning rate of the 30 escape responses used in analysis was $1166 \pm 389^\circ\ s^{-1}$, which clearly distinguished them from spontaneous turns (with turning rates $357 \pm 103^\circ\ s^{-1}$, n = 20). Spatial XY coordinate data, along with depth as determined from side-view videos, with data taken from calibration videos were used to determine the distance of the fish from the screen at the moment of the response.

For each escape response the frame of the looming animation at which the response was initiated was used to identify the associated $d\alpha/dt$ (the apparent LT) at which the

response occurred in the relevant attack scenario model. The calculated dα/dt in each attack scenario assumed a viewing distance of 16 cm when used to create the looming animation, but actual fish distances to the screen varied slightly from this, which affects the actual dα/dt experienced. To minimise this variability only responses which occurred 3 cm to either side of the hypothesised 16 cm viewing distance were used, and the dα/dt of each of these responses was adjusted for the viewing distance using the relationship:

$$\alpha = 2 \times \operatorname{atan} \frac{0.5 \times stimulus\ diameter\ on\ screen}{screen\ distance}$$

resulting in a mean apparent LT_{exp} of 2.05 ± 0.49 rad s^{-1}. Accounting for visual response latency (see below) resulted in a mean true LT_{exp} of 1.66 ± 0.37 rad s^{-1} (Table S1). The same calculations of α and dα/dt were applied to the response prediction models that utilized both metrics (Fig. S4).

Determination of visual response latency in anchovies

There is a lag between the brain sensing a stimulus and the body initiating a movement (6, 7, 10, 16). Looming animations continuously increase and as such do not typically provide an instantaneous moment of disturbance from which to measure neural lag, so to determine the actual dα/dt value of a response some assumed latency value must be applied. To estimate the latency between a visual stimulus and a physical response in *E. mordax*, experiments in which they were exposed to a sudden camera flash were conducted. Twelve trials were conducted in which individual anchovies were moved to a 1.5 m diameter tank. After 30 minutes, they were exposed four to five times to a camera flash, separated by 5 to 10 minute intervals, and filmed at 120 FPS using a GoPro Hero 4. Videos were reviewed for potential responses to the flash, characterized by either a sharp lateral turn, or rapid dash away in the direction of swimming. The frame at which the flash occurred was identified, and the video progressed frame by frame to identify how many frames after the flash that the initiation of the response was apparent. This was converted to a minimum latency duration in milliseconds. Of the 12 fish, nine showed a response to at least one flash. Those that responded to more than one flash (3 of the 9) were relatively consistent in their response times, varying by 2 frames (17 ms), 1 frame (8 ms), and 0 frames. For these three fish a mean latency between the two responses was calculated, for all others the single response latency was used, giving one latency value for each fish. The resulting distribution ranged from 33 to 88 ms and was non-normal (Shapiro-Wilk normality test, $n = 9$, $p = 0.005$), thus we applied the median latency value (61 ms) to calculated LT values.

Responses to the looming animations

All specimens in the AF and KF trials responded shortly after dα/dt increased abruptly, the moment of apparent mouth opening (AMO) simulating where the viewing angle (α) of the rapidly opening mouth surpasses that of the maximum girth (Fig. S5). Assuming a minimum response latency of 33 ms, the lower end of the range estimated in the response latency estimation experiments, all responses occur after this moment (Fig S2, column 2). Any single latency value higher than this applied to all specimens, e.g. the mean or upper end of the range established in the response latency estimation experiments (61

and 81 ms respectively), would mean some specimens appear to respond before the mouth opens. However, since we did not see any responses in the constant speed (CS) trials at $d\alpha/dt$ values this low (< 0.23 rad s^{-1}), the parsimonious explanation is that these specimens are instead responding at latencies on the low end of the calculated values (~33 ms). Overall, the placement of responses in these two scenarios are consistent in suggesting that fish are responding to a similar LT range as established in the CS scenario. Moreover, they illustrate how the characteristics of whale attacks compress the range of LT_{exp} into a very brief moment at apparent mouth opening, such that any escape response by the targets to values in the LT_{exp} range will occur within a brief, predictable temporal window during the attack.

This finding of a narrow temporal window encompassing the calculated response thresholds but a relatively wide range of response times after the stimulus threshold is passed differs from previous work largely due to the nature of the approach stimulus. That is, previous work that used looming approaches to trigger escape employed stimuli that changed size smoothly whereas our approaches were constructed from measured predator data and had a defining point of inflection with a rapid increase in stimulus size coincident with mouth opening. This rapid increase is similar in effect to an approaching predator that exhibits sudden accelerations. Our results suggest that fish may have delayed responses to such events, which may in turn explain why many predators, such as sea lions and whales, do not approach schools using smoothly increasing speeds but instead vary their speed and attack angles within an approach.

The variation in response timings after AMO, which was as high as 300 ms (Fig. S5), is not fully explained by individual variation in visual response latency which we observed to range from 33 to 88 ms. To investigate further properties of the stimulus that may influence response reactions, we additionally investigated if response models based only on stimulus size (α) regardless of attacker speed would explain the results (17). However, the α values for AF/KF at response were significantly lower ($p = 0.002$) than in the CS trials, which made it clear that this was not a credible response model. Next we investigated if response models based on the rate of increasing stimulus size ($d\alpha/dt$), but that incorporated an inhibitory function of α (18, 19) would better explain the observed responses than models based only on $d\alpha/dt$. All of the models tested had similar variability in response timing (200-400 ms) (Fig. S4), so none of the models better explained the observed variation (Fig. S4). Therefore, when the response models were applied to attack simulations to calculate catch percentages (see below), both a "quick response" scenario using the median visual response latency (61 ms) and a "slow response" scenario with an additional 200 ms delay were used to bound the predictions of how many anchovies could be captured by a lunge feeding event.

Anchovy escape speeds

To determine the speeds at which anchovies flee, laboratory trials were conducted in which small groups were filmed in a large tank escaping from a mechanical stimulus (the far end of a broom handle touching the surface of the water), and the acceleration and speed of individuals (n = 12) was determined over 1 s to 1.33 s (Fig. S6). Typical escape swimming behavior was a rapid acceleration from almost stationary to between 2 and 3 m s^{-1} in approximately 0.3 s (consistent with other fish within this size range (15, 20)), followed by maintenance of this speed or slight deceleration. Maintenance of initial burst

speeds for ~ 1 s is common in non-pelagic species (21) before deceleration to ~ 1/2 speed. In our case, because the natural deceleration could not be separated from deceleration because of the tank walls, the final speed was assumed to be maintained through the duration of a humpback's gape cycle. The fastest mean fish, and the mean of all fish were used separately as inputs into the model.

Simulations of capture efficiency

The min (0.89 rad s^{-1}), mean (1.66) and max (2.06) LT_{exp} of response, and the min, mean and max anchovy escape speeds (Fig. S6) for five different escape trajectories that encompassed the range of theoretical responses (see below) were used to construct the probabilities that fish in a school would escape from an approaching 10.5 m humpback whale with max girth 2.5 m located 4.41 m behind the front of the whale with 2.25 m jaws (the same whale size assumed in the looming threshold experiments). For results reported in Figs. 3 & 4 we assumed that anchovies fled the predator at the mean escape speed observed in the lab (accelerating from 0 to 2.3 m s^{-1} in 0.3 s and maintaining that speed through the escape, Fig. S6). While a humpback whale's shape can be approximated by a cone with the maximum girth visible to the prey for most of the approach (Fig. 1A), at close viewing distances (< 1 m) the maximum perceived projection of the whale may instead be a part of the animal more anterior than the maximum girth. These real-life shapes were accounted for in simulations of fish responses to predator approaches, and the non-ideal shape of humpback whale, blue whale and sea lion predators were estimated from profile and overhead images of each species. These shape parameters are reported in the supplemental R and Matlab codes.

The tested approaches followed the mean Type 1 and Type 2 speed and engulfment profiles shown in Fig. 4, with mean engulfment calculated as distance from the first inflection point of the speed profile after the max speed. We constructed models assuming both that fish responded directly to the stimulus of the approaching whale or would respond instead to the reactions of the fish around them (22). In the second case, the response was modeled as if the school responded in a wave moving away from the initial stimulus at 6.7 m s^{-1} (23). Any fish located more than 24 cm (two body lengths) away from the edge of the school was assumed to respond to the school as the line of sight to the approaching predator was likely obstructed. To encapsulate the observed variation in humpback whale approaches, in the model tests we alternately varied the distance from the school at which the whale would open its mouth, the timing of the mouth opening event along the speed profile, and also multiplied the speed of the SoCal approach by factors from 0.1 to 3. In all cases, the timing of maximum engulfment and overall engulfment duration were scaled using calculations from (2) such that the overall volume of water engulfed would be consistent.

For any given humpback whale engulfment profile α and $d\alpha/dt$ were calculated from the viewpoint of theoretical target fish at every time step (at 60 Hz) along the whale's approach using the LT model (Code S1). Then, for a given LT at which the fish respond, the time from the whale reaching this LT for each fish in a school to when the whale's jaws would reach the fish was calculated for each of 5 different potential prey escape trajectories:

1) A perpendicular escape trajectory in which all fish flee in a direction directly perpendicular to the oncoming whale's trajectory
2) Like #1, but assuming that all fish fleeing laterally are flushed back towards the mouth by the flippers (24, Movie S4) and consumed. We calculated the percentage of fish that would additionally be caught if fish fleeing to the outside of the school perpendicular to the whale's path were instead corralled by the flippers back towards the mouth and engulfed (Figs. 2d, 4). In this scenario, at least 50% of fish would be caught every time. This appeared to be the least realistic scenario.
3) An angled escape calculated from the instantaneous ratios of the whale's speed and the anchovy escape speed as $180° - \text{acos}(U_{prey}/U_{pred})$ (25), where 180° is directly away from the predator. These values varied from 101° to 180° (either to the left or right) and are the most likely initial escape trajectories based on published work on clupeoid fish (25-27).
4) Like #3 but with the horizontally fleeing fish flushed back towards the mouth
5) An escape directly away from the oncoming whale along the same trajectory. In this scenario if the whale is faster than the fish, all fish are engulfed, and if the whale is slower all fish escape.

The "escape distance" each fish would be able to travel perpendicular to the whale's approach in the time before it was reached by the whale's jaws was calculated. For every fish in a disc perpendicular to the whale's attack, their "safe distance" was the distance that fish had to travel horizontally (perpendicular to whale approach) to be outside a space the area of the whale's jaws. If a fish's escape distance did not exceed the safe distance, the fish was assumed to be engulfed. The percentage of fish at each time step that could escape was then summed and standardized for the size of the whale's mouth at each time step, and a total catch percentage was calculated. As escape scenarios 3 & 4 are the most likely scenarios, they are reported in Figs. 2-4. Other escape scenarios had increased catch percentages but similar trends in the importance of timing. Similarly, only the scenario using mean LT_{exp} is reported in the figures, but no substantial differences were found when using min or max LT_{exp} as all were nearly coincident in all models where the whale opened its mouth.

For all catch percentage simulations run, the size of the fish school was assumed to be larger than the engulfment volume of the whale such that if the fish did not flee, the whale's mouth would be full of fish at their schooling density. At each time step, fish in the school were assumed to be evenly distributed in a plane perpendicular to the oncoming whale in two semi-circles – one with radius of the vertical projection of the upper jaw at that time ($Length_{jaw} \times \sin(JawAngle)$) and one with radius of the vertical projection of the lower jaw.

For results presented in Figs S1 and S2, the escape responses of fish to the LT_{exp} was compared to the escape responses given a model that assumes an inhibitory effect of loom size (α) using the equation $\eta = \alpha \times e^{-2.576\,\alpha'}$, where $\alpha' = d\alpha/dt$ (see Fig S4 for details on model construction). Figs S1 and S2 also model catch percentages assuming that fish respond in the wild nearer to the slower responses we observed to AMO. Catch percentages thus range between the maximums for the quicker and the slower observed responses.

Additional predator capture efficiency

To compare how anchovy escape responses to attacking humpback whales compares to both larger whales and to particulate feeding predators, varying size inputs and speed/engulfment profiles were input into the dα/dt profile code (Code S1). For the blue whale simulation, we used the mean speed profile from (2) and a mid-sized 22.8 m long blue whale with 3.1 m girth diameter and max girth placed 20% behind the rostrum. For a predator foraging on single prey, we simulated the California sea lions (*Zalophus californianus*) observed to feed in concert with the whales in this study (Movies S1, S2, S4). We measured a medium sized sea lion from overhead imagery as 1.67 m with 0.55 m girth diameter located 32% of body length behind the snout. An average sea lion has jaws 6.3 ± 1.4 cm wide (28) which can be used to interpret the likelihood of a fish's escape. Although the approach speed of sea lions is not precisely known, we chose constant approach speeds (3.5 and 5.5 m s^{-1}) that span the range of typical to extreme sea lion speeds (29, 30), as well as the approach profile of a blue whale to examine how the influence of size alone affects anchovy perceptions of predators.

Given these inputs, we calculated when an approaching predator would exceed the mean LT_{exp} for a fish that is initially located at the spot at which a whale would reach maximum gape or at which a sea lion would reach maximum speed. For the whales, catch percentage was determined as above. For the sea lion, horizontal escape distance of the fish was calculated by determining the ideal escape angle for the fish to flee as in scenario (3) above, a latency of 61 ms was applied, and then the mean escape speed as well as the mean ± 1 SD escape speeds were applied. Results are displayed in Fig. S7. In all sea lion cases, the LT of anchovy response occurred before the sea lion would arrive at the fish. In all whale cases, the LT of response occurred after the whale would have already opened its mouth.

Humpback whale foraging efficiency

The surplus efficiency of a lunge (Fig. 4) was calculated as $(E_{in} - E_{out})/E_{out}$. Estimates of metabolic expenditures (E_{out}) are based on calculating the energy spent by the locomotor and ventral groove blubber (VGB) musculature during the energetically most significant stages of a feeding lunge, namely pre-approach and engulfment as detailed in (31). These calculations are based on the use of tag data as input in a calculation of the mechanical energy, which is then corrected by propulsive and metabolic efficiency constants to yield the sought-after metabolic expenditures (32-36). The mechanical expenditures by muscle are obtained from the work-energy theorem applied to the whale's body in which changes in kinetic energy are expressed in terms of the energy loss through drag generation and/or gained via fluking. This approach has been used previously for estimating the energetics of the engulfment stage during lunge-feeding for krill by blue whales (37), and has been generalized to include fluking-induced accelerations in both prey-approach and engulfment stages (as detailed in 31). Energy during acceleration was thus determined as $\frac{\Delta KE}{\gamma_1\gamma_2} + robMR \times (t_2 - t_1)$, any coasting or deceleration from drag was $robMR \times (t_2 - t_1)$, and any work done during engulfment by the VGB was $\frac{M_c}{2\gamma_1\gamma_3}(v_{higher}^2 - v_{lower}^2)$, where ΔKE takes into account any changes of mass from engulfment, γ_1= metabolic efficiency (0.25), γ_2 = propeller efficiency (0.8), γ_3 = extra muscle use efficiency (0.9), *robMR* = Rest of body metabolic rate = $1.6 \times 4.1\, M_c^{0.75}$ (31,

38, 39), t_2 and t_1 are the times (in s) at the end and the beginning, respectively, of the period of interest, M_c is the mass of the cetacean (pre-engulfment) and v_{higher} and v_{lower} are the start and end velocities, respectively, during deceleration or the end and start velocities during acceleration. M_c was calculated using the ordinary least-squared scaling equation for a 10.5 m whale (11). Matlab code to calculate energy expenditure from speed and engulfment data is available as Code S2, and as a first approximation, the overall energy used by foraging humpback whales can be estimated using a quadratic model ($r^2 = 1.000$): $E = 0.01966x^2 + 0.1066x + 0.3895$ where E is energy in MJ and x is maximum speed of the lunge (Fig. 3a).

For all scenarios, the energy from successfully engulfed prey (E_{in}) was calculated as $E_{in} = V_{engulf} \times fish\ density \times energy\ density$, where V_{engulf}= engulfed water mass (11) divided by the density of sea water (1027 kg m^{-3}), and a representative *fish density* of 7.8 kg of fish per cubic meter of water (based on length-weight relationships from (40), a school packing density of 1 body length cubed per fish (41, 42), and a representative fish length of 12 cm) and *energy density* of 6 MJ/kg (43, 44). This value was then scaled by the percentage of fish caught (Fig. 3).

For the Type 1 whales that utilized high speed approaches to dolphin-associated schools that were typically smaller than a whale's engulfment volume, the mean school size was generally smaller than a whale, averaging ~ 1 m in diameter (the length of a common dolphin, Movie S2). A scaling factor of 29% could thus be applied to E_{in} (and then applied to the storage efficiency equation) for applications in energy acquisition modeling. Because the point of these exercises was to compare the engulfment energetics of different engulfment scenarios, this scaling factor was not applied in Figs 3 and 4.

Humpback whale AF and KF feeding rates

To compare foraging rates of AF and KF whales, we identified all lunge-feeding events from the tag records of the AF whales in this study as well as seven additional KF humpback whales from Monterey Bay, CA tagged 2016-2018 using CATS tags. Lunge rates from these seven were combined with lunge rates from 4 other published records in California (2, 45). Only California whales were used for comparison to AF whales so as to include only sympatric whales that could theoretically choose to feed on anchovies or on krill. Lunge-feeding events were identified from the tag records as peaks in speed with rapid deceleration (2) that correspond to increases in |jerk| (46) as well as changes in pitch, roll and heading associated with maneuvering. Reported results are feeding rates for the duration of the AF deployments all of which only spanned daylight hours (mean deployment time: 3.3 ± 2.6 hrs, max: 7.9 hrs). KF deployments were broken into daylight or night time to account for diurnal variation in feeding behavior and reported results are the means of either daylight feeding rates for (10 of 11 deployments that were daylight feeding dominant) and the night time feeding rate of the whale that was night time feeding dominant. For comparisons of E_{in} between AF and KF lunges, anchovy parameters were as in the storage efficiency calculations, and krill patches were assumed to be consumed with low escapement (90% catch), to have an energy density of 3.8 MJ kg^{-1} (47) and to be engulfed at an approximate average density (1 kg m^{-3}) observed from echosounder data in California collected concurrently with tagged KF whales.

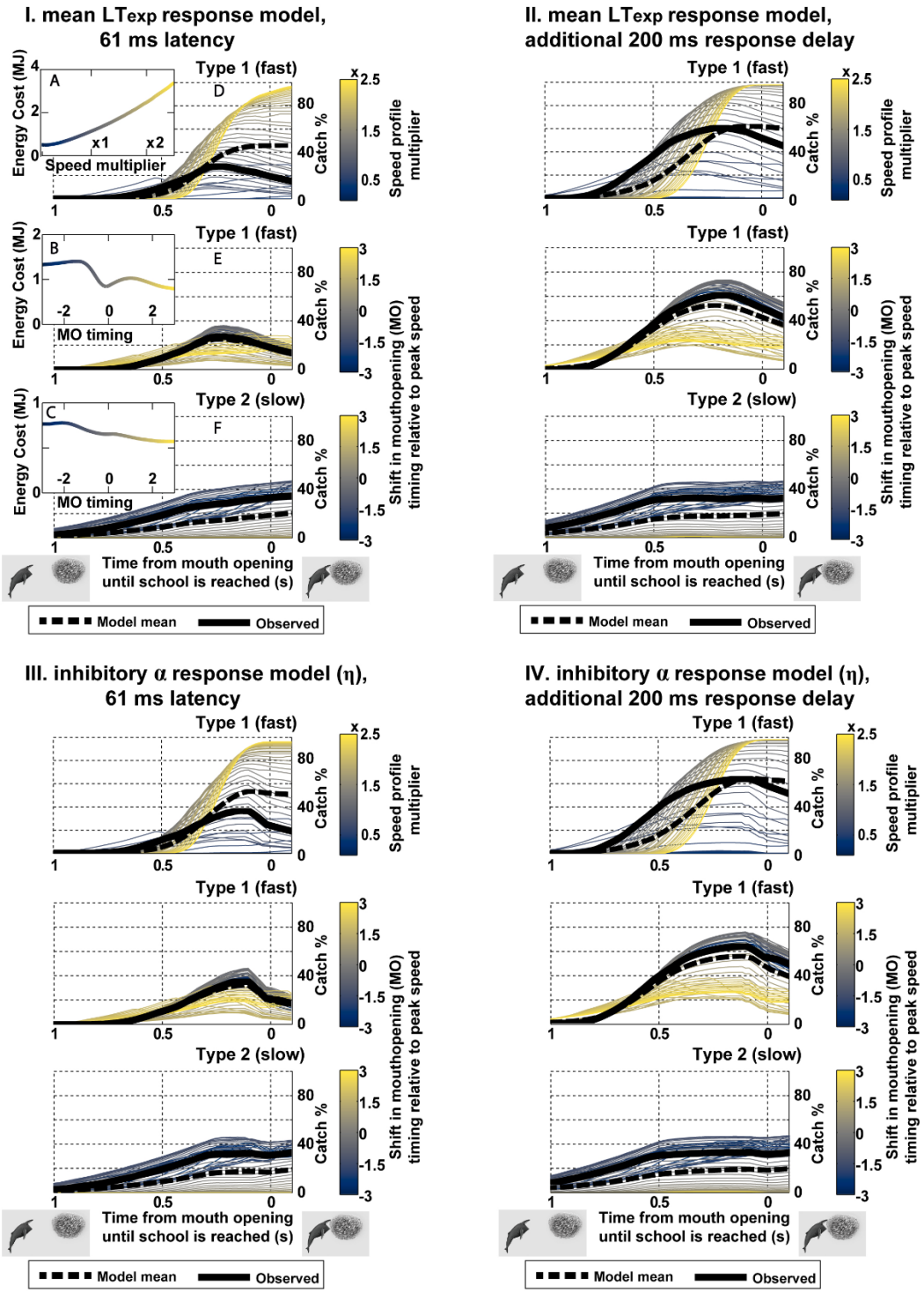

Fig. S1- Modeled catch percentages based on different response scenarios. See Fig. 3 caption for more details. I) same as Fig. 3. This is the dα/dt threshold with 61 ms latency applied. II) The dα/dt threshold model with 261 ms latency applied. This is the maximum expected catch if fish respond in the wild at the slower responses observed in the lab. III) Modeled catch percentage assuming the response to looming rates are inhibited at large α (η model described in Fig. S4). IV) Modeled catch percentage for the η model and using a 261 ms latency.

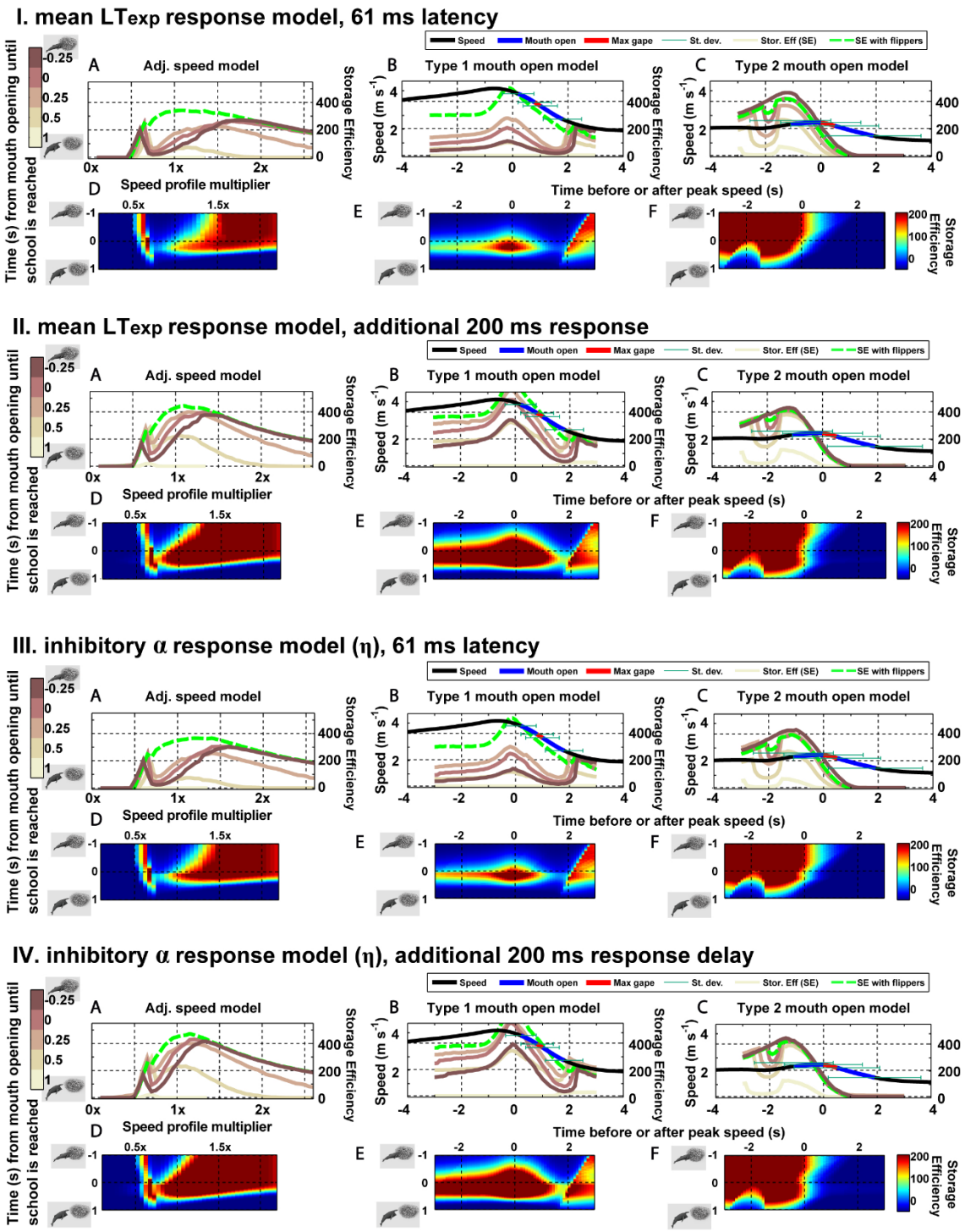

Fig. S2- Modeled foraging efficiencies (surplus efficiency) based on different response scenarios. See Fig. 4 caption for more details. I) same as Fig. 4. This is the dα/dt threshold with 61 ms latency applied. II) The dα/dt threshold model with 261 ms latency applied. This is the maximum expected catch if fish respond in the wild at the slower responses observed in the lab. III) Modeled catch percentage assuming the response to looming rates are inhibited at large α (η model described in Fig. S4). IV) Modeled catch percentage for the η model and using a 261 ms latency.

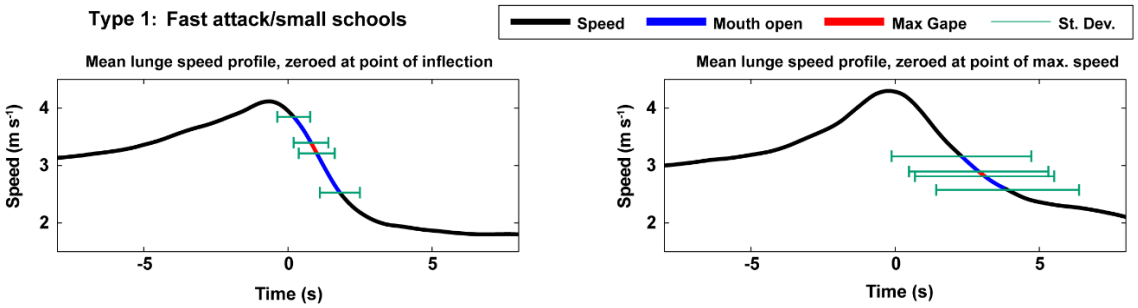

Fig. S3- The engulfment timing and speeds of tagged anchovy-feeding whales in SoCal were faster and more consistent in timing than previously reported fish-feeding humpback whales, and were similar in character, with engulfment consistently coincident with the rapid deceleration phase, to previously reported krill-feeding rorquals (2). A) the mean speed profile (also displayed in Fig. 1 and Fig. 4B) of 84 lunges from 9 whales, centered around the timing of rapid deceleration onset where mouth opening is 0.2 ± 0.6 s after this point of inflection. In many cases, this point was not coincident with peak speed as many whales started decelerating before mouth opening. B) When the same data are centered around peak speed, engulfment timing is much more variable, implying that the point of inflection is a result of deceleration from the high drag of engulfing a water mass that can exceed body mass (11).

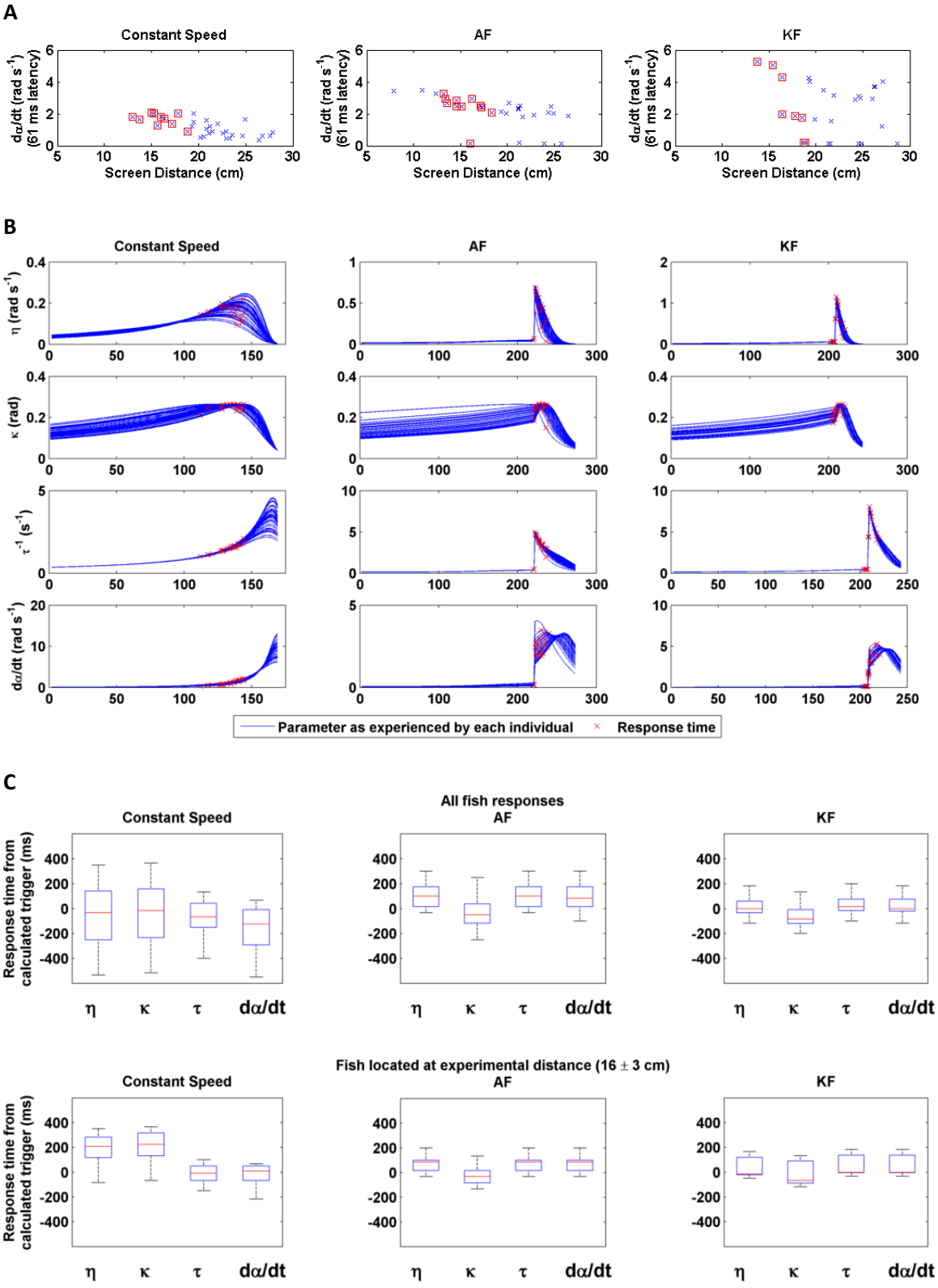

Fig. S4- Summary of stimulus response interpretation models, as formulated in (19). In all panels, $\alpha' = d\alpha/dt$, $\eta = \alpha \times e^{-2.576\,\alpha'}$, $\kappa = \alpha \times e^{-1.393\,\alpha}$, $\tau^{-1} = \alpha'/\alpha$ and all panels applied a

neurological latency of 61 ms. The constants in the formulations of η and κ were derived by finding the global value that minimizes the squared difference in the time of the observed responses during the constant speed experiment from the maximum of the curves. A) LT of response for every fish in all three playbacks as a function of distance from the screen. The decreasing slope of responses suggests that response to dα/dt may be inhibited by larger α. Only data points with red boxes (fish within 3 cm of the intended 16 cm distance) were used in further analyses. B) Responses of each fish plotted on its observed line (lines differ based on different screen distances). C) Variation in anchovy response timing for all three stimulus experiments using all four stimulus interpretation models. While there is slightly less variation in the τ and dα/dt threshold based models in the constant speed experiments, no model does a better job of explaining the variation in response timings in the real approach speeds, suggesting there are additional factors besides loom rate (dα/dt) and loom size (α) that influence response timing.

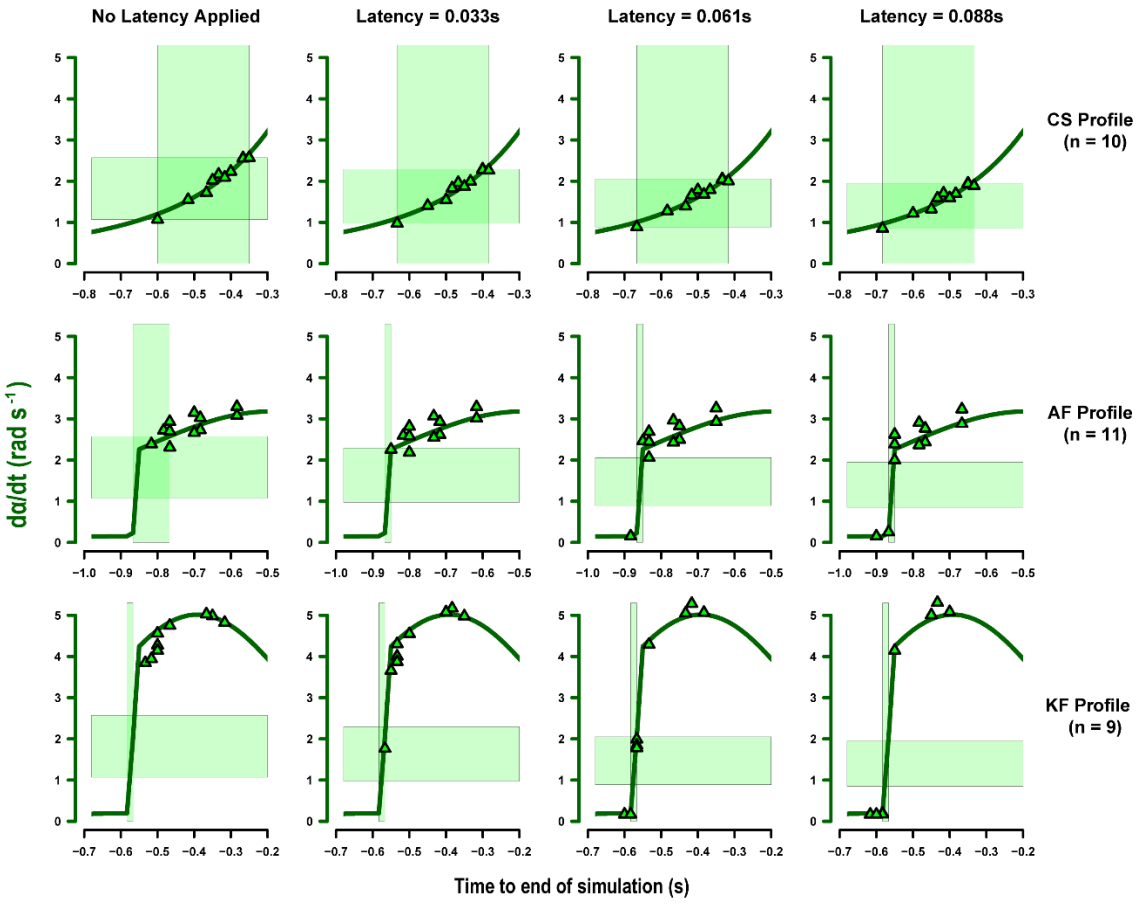

Fig. S5- Anchovy escape response timings (triangles) in each of the three looming animation trials (CS = constant speed, AF = anchovy feeding, KF = krill feeding) in relation to dα/dt with the experimental range of neural response latency values applied. Horizontal axes represent a 0.5 s window containing all responses. The green line represents changes in looming stimulus dα/dt as observed from the assumed viewing distance of 16 cm (only fish that were within 3 cm of this distance at the time of response were included in our analyses). Vertical offset of points from this line result from corrections to each fish's observed dα/dt due to deviations from the assumed viewing distance. Green shaded regions indicate the lower to upper range of LT_{exp}, based on applying that column's latency to the CS profile, as well as the time period over which this occurred. In the CS trials this range occurs over approximately 0.25 s while in the trials modelled from whale kinematic and engulfment data, it is compressed into a single animation frame once latency is applied. The potential for delayed responses to stimulus crossing is apparent in the AF and KF trials as some fish responded 200-300 ms after AMO. The delayed response models in Figs. S1 and S2 account for the potential for these longer response times to be conserved in the wild.

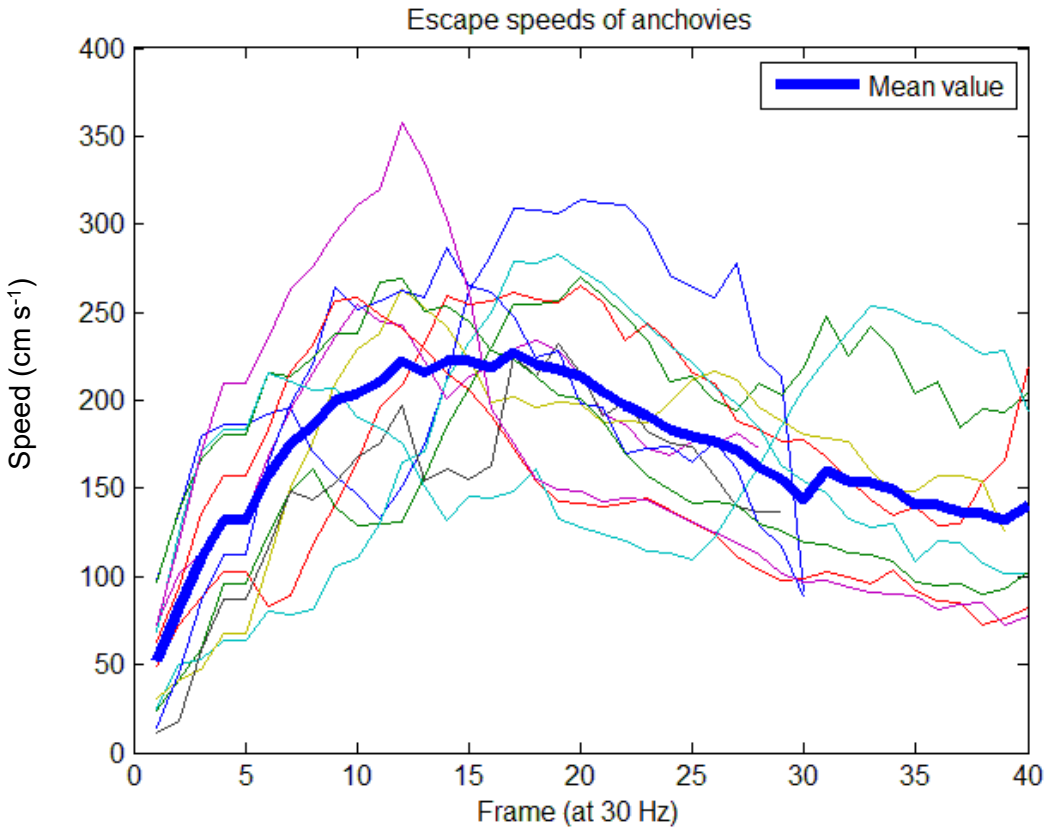

Fig. S6- Speeds of 12 anchovies fleeing a mechanical stimulus recorded with a high speed camera.

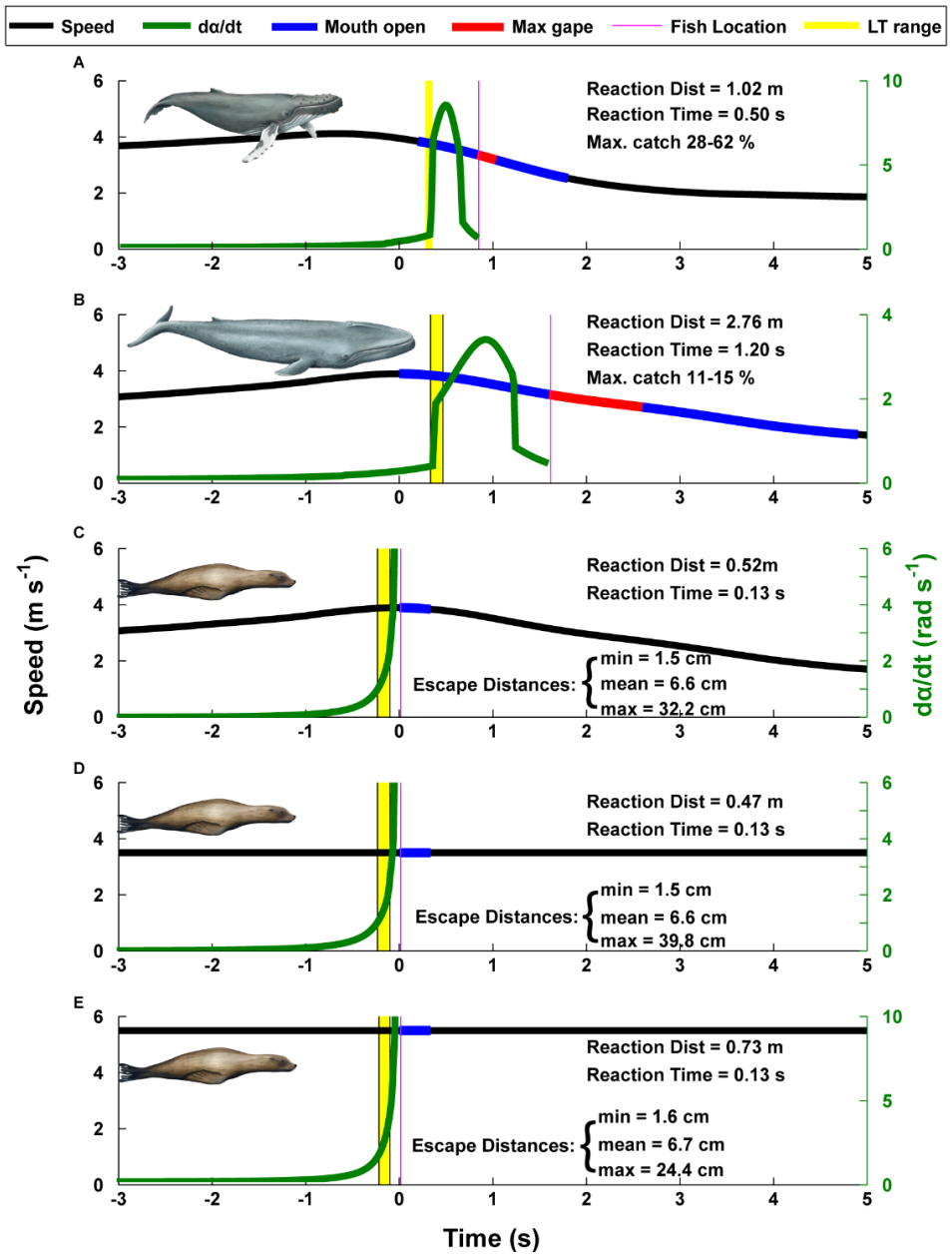

Fig. S7- Approach simulations based on speed (black) and mouth opening (blue/red) that result in looming stimuli changing size at dα/dt (green). A) The Type 1 humpback approach profile- min/mean/max LT_{exp} are all reached simultaneously for a fish that would be reached at maximum gape, but after the whale has already opened its mouth. Max catch range is based on slow and fast response times (Fig. S5). B) A simulated blue whale approach, the long engulfment time means more fish have a chance to escape. C) A sea lion approach using a blue whale speed profile but with a sea lion's size. D) A constant speed (3.5 m s^{-1}) approach of a sea lion sized predator. E) A faster constant speed sea lion approach (5.5 m s^{-1}). In sea lion scenarios, all LT_{exp} are reached before the sea lion reaches the prey. Escape distances are how far an anchovy would be able to travel horizontally before being reached by the jaws of the sea lion. Min = late detection (max LT_{exp}) and slow escape (mean fish escape speed – 1 SD), mean = mean LT_{exp} and mean escape speed, max = early detection (min LT_{exp}) and fast escape (mean + 1 SD).

Table S1- Anchovy looming stimulus experimental results of fish that were within 3 cm of the assumed 16 cm screen distance (30 fish total). CS = constant speed, AF = anchovy feeding, KF = krill feeding. A looming stimulus that represents a predator typically gets bigger by getting closer to the prey, however a rorqual whale has an uncommon approach in that it also expands its profile when the jaws extend past the maximum girth at apparent mouth opening (AMO), implying that an anchovy may perceive this threat as approaching much more rapidly (final column) than the modeled speed. (1) Distance from screen at moment of response (cm), (2) Time from AMO until response (s), (3) Apparent LT of response ($d\alpha/dt$ in rad s^{-1} corrected for screen distance), (4) True LT of response ($d\alpha/dt$ in rad s^{-1} after applying median neurological latency), (5) Modelled speed (m s^{-1}) at moment of response (0 latency), (6) Perceived speed (m s^{-1}) at moment of response (0 latency). If results for fish not within 13-19 cm of the screen (<13 cm, n = 3, >19 cm, n = 57) are included in analysis, no substantial difference in timing of response was noted (fish still respond within ms of the AMO event).

Specimen	Scenario	(1) Distance from screen (cm)	(2) Time from AMO (s)	(3) Apparent LT (rad s^{-1})	(4) True LT (rad s^{-1})	(5) Modelled speed (m s^{-1})	(6) Perceived speed (m s^{-1})
CS01	CS	13.02	n/a	2.16	1.79	5.0	4.1
CS02	CS	13.75	n/a	2.02	1.66	5.0	4.3
CS03	CS	15.00	n/a	2.56	2.06	5.0	4.7
CS04	CS	15.22	n/a	2.55	2.04	5.0	4.8
CS05	CS	15.67	n/a	1.55	1.28	5.0	4.9
CS06	CS	16.03	n/a	2.24	1.79	5.0	5.0
CS07	CS	16.36	n/a	2.09	1.68	5.0	5.1
CS08	CS	17.20	n/a	1.72	1.39	5.0	5.4
CS09	CS	17.86	n/a	2.57	2.00	5.0	5.6
CS10	CS	18.80	n/a	1.07	0.89	5.0	5.9
AF01	AF	13.18	0.27	3.29	3.26	2.1	5.3
AF02	AF	13.34	0.15	3.15	2.97	2.2	9.3
AF03	AF	13.55	0.08	2.93	2.69	2.2	14.0
AF04	AF	14.54	0.07	2.72	2.46	2.2	16.8
AF05	AF	14.61	0.17	3.03	2.83	2.2	9.4
AF06	AF	15.08	0.08	2.70	2.45	2.2	15.6
AF07	AF	16.03	0.03	2.39	0.15	2.2	23.4
AF08	AF	16.26	0.27	3.08	2.93	2.1	6.6
AF09	AF	17.17	0.17	2.73	2.50	2.2	11.0
AF10	AF	17.22	0.15	2.67	2.43	2.2	12.0
AF11	AF	18.30	0.08	2.31	2.06	2.2	18.9
KF01	KF	13.71	0.22	4.98	5.28	2.6	6.0
KF02	KF	15.38	0.25	4.82	5.07	2.6	5.5
KF03	KF	15.42	0.20	5.03	5.05	2.6	7.5
KF04	KF	16.37	0.07	4.56	1.99	2.7	23.7
KF05	KF	16.43	0.10	4.75	4.29	2.6	17.0
KF06	KF	17.81	0.07	4.27	1.84	2.7	25.8
KF07	KF	18.51	0.07	4.14	1.78	2.7	26.8
KF08	KF	18.66	0.03	3.84	0.17	2.7	40.0
KF09	KF	18.90	0.05	3.94	0.17	2.7	33.0

Movie S1- Anchovy schools disperse when attached by humpback whales, while krill schools do not show an apparent escape response. Although this is a single example, coordinated escape by krill has not been observed in any of hundreds of lunges from whale-borne camera footage. High-quality version available at: https://purl.stanford.edu/mt574ws5287

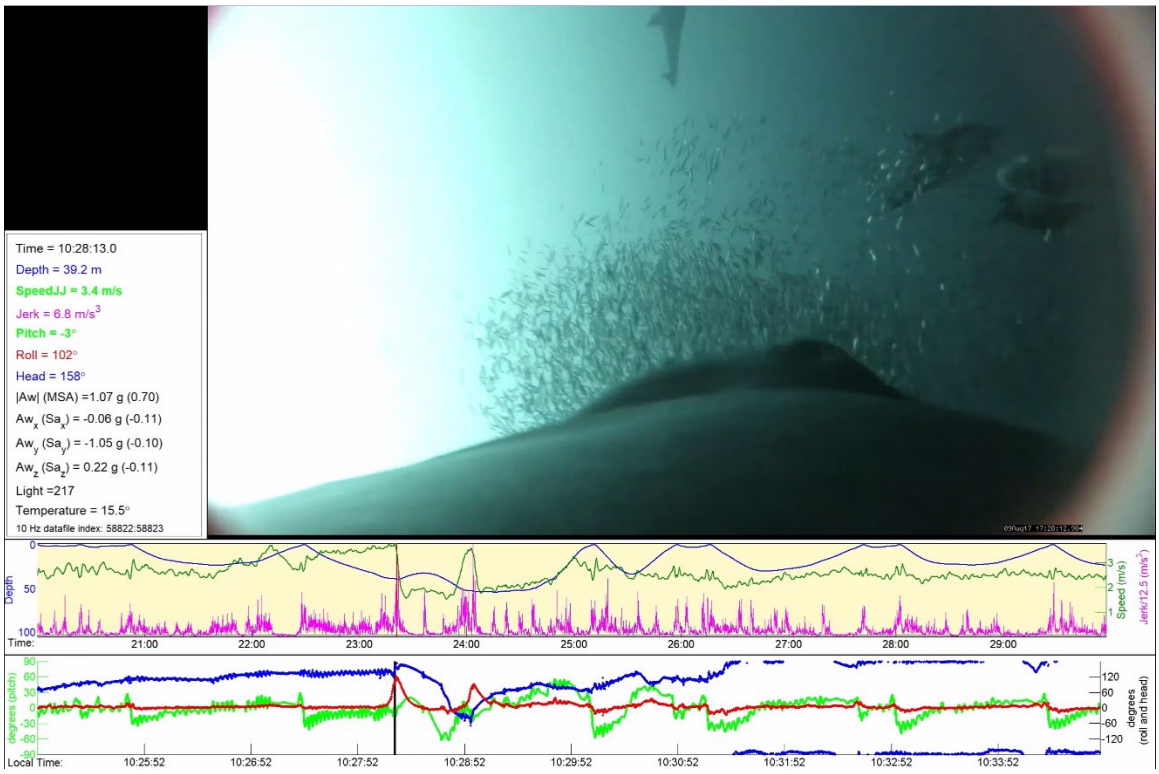

Movie S2- Humpback whales in the study from Southern California (SoCal) fed at high speeds on small schools in concert with common dolphins (*Delphinus sp.*). A humpback whale from Monterey Bay, California fed at slower speeds on a large school in concert with California sea lions (*Zalophus californianus*). High-quality version available at: https://purl.stanford.edu/mt574ws5287

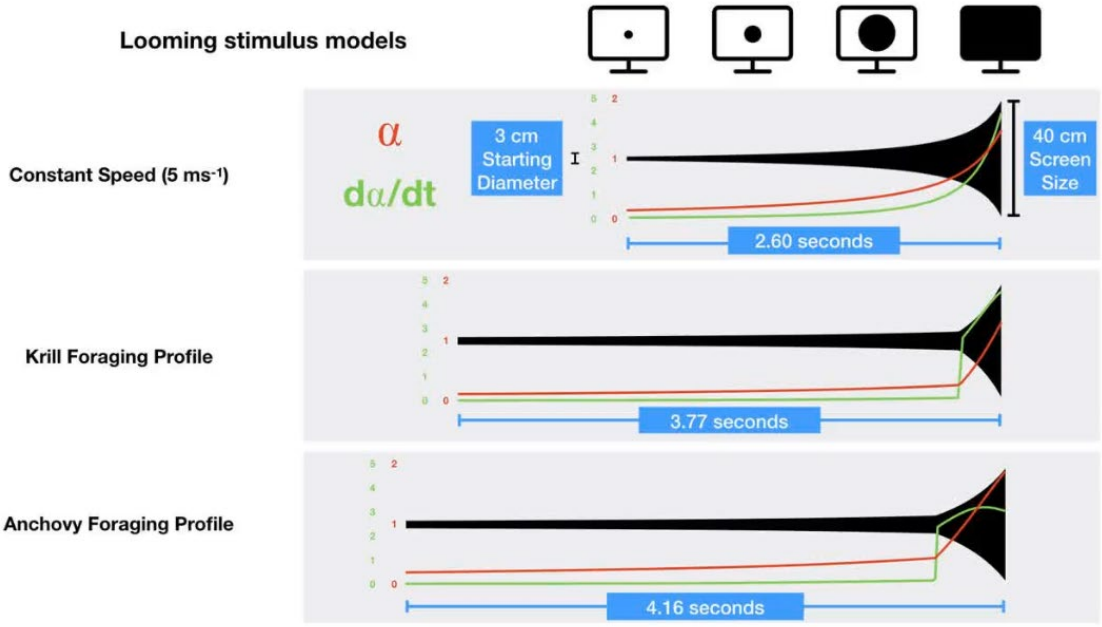

Movie S3- The visual stimuli used to test the escape responses of anchovies (*Engraulis mordax*). The stimuli parameterized from predator data had delayed and then rapid expansion of the stimulus. Times in the screenshot above refer to times from the start of the simulation until the screen is completely filled.

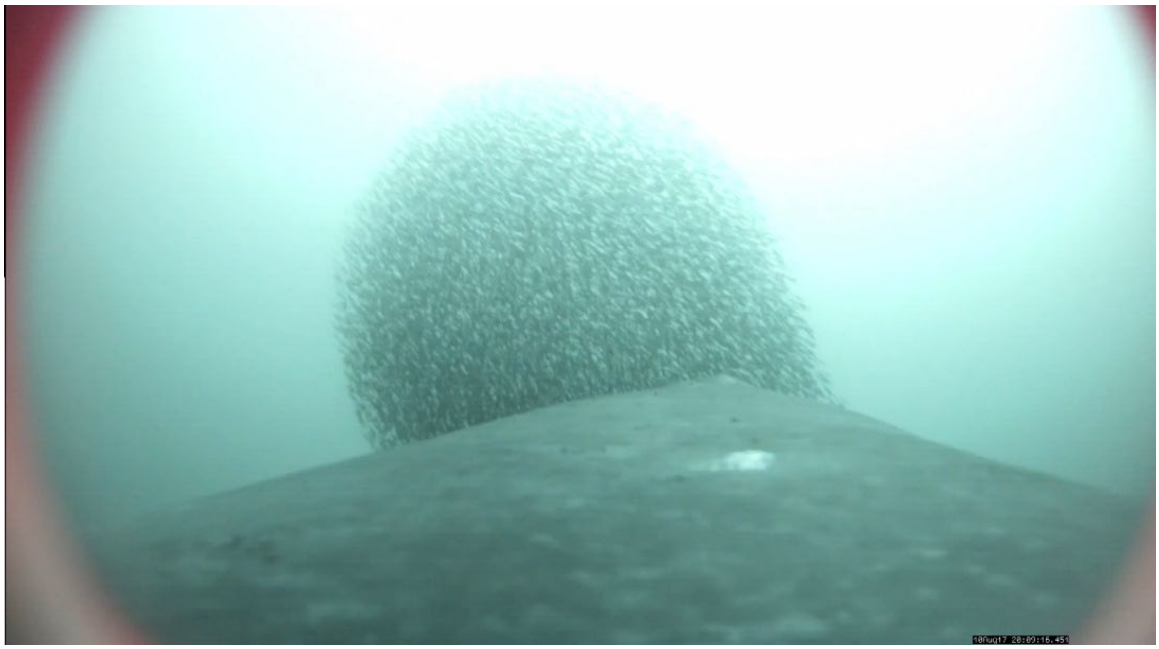

Movie S4- Humpback whale flippers are extraordinarily long (~ 30% of body length (11)) with white bottoms, and attacking whales regularly rotate and extend them when lunge-feeding, a technique that has been shown to have a startle effect on prey (24). When humpback whales approach prey but do not open their mouths, schools maintain formation since the threshold of response is not reached. High-quality version available at: https://purl.stanford.edu/mt574ws5287

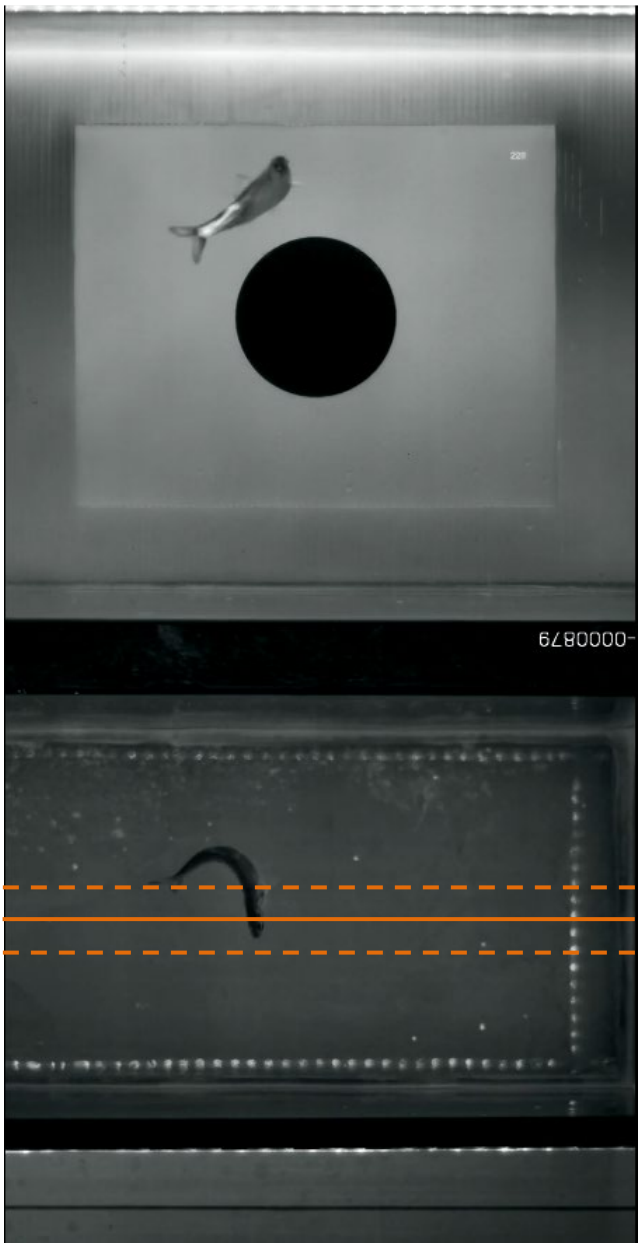

Movie S5- An anchovy (AF04 from Table S1) demonstrates a characteristic c-start escape response away from the stimulus when startled. High-speed cameras (250 Hz) allowed precise determination of the timing of response, and the frame number in the corner of the playback screen showed the stage of the animation at which the response occurred. In the overhead view the stimulus playback screen is situated along the top of the frame, the thick line was added to this image to represent the middle of the tank (16 cm from the screen), and the dotted lines represent the screen distance range (± 3 cm) at which a fish's response must occur to be counted in our analysis.

Supplemental code

The following scripts are available for download at:
https://purl.stanford.edu/mt574ws5287

Code S1 (in R and Matlab) to create the looming stimulus based on predator size, speed and engulfment timing

Code S2 (Matlab) to calculate energetic output of a lunge-feeding whale from speed and engulfment timing

Supplemental References

1. Cade DE, Carey N, Domenici P, Potvin J, & Goldbogen JA (2019) Data for "Predator-informed looming stimulus experiments reveal how large filter feeding whales capture highly maneuverable forage fish". Stanford Digital Repository. (https://purl.stanford.edu/mt574ws5287).
2. Cade DE, Friedlaender AS, Calambokidis J, & Goldbogen JA (2016) Kinematic Diversity in Rorqual Whale Feeding Mechanisms. *Current Biology* 26(19):2617-2624.
3. Goldbogen JA*, et al.* (2017) Using Digital Tags With Integrated Video and Inertial Sensors to Study Moving Morphology and Associated Function in Large Aquatic Vertebrates. *The Anatomical Record* 300(11):1935-1941.
4. Johnson MP & Tyack PL (2003) A digital acoustic recording tag for measuring the response of wild marine mammals to sound. *IEEE Journal of Oceanic Engineering* 28(1):3-12.
5. Cade DE, Barr KR, Calambokidis J, Friedlaender AS, & Goldbogen JA (2018) Determining forward speed from accelerometer jiggle in aquatic environments. *Journal of Experimental Biology* 221(2):jeb170449.
6. Batty R (1989) Escape responses of herring larvae to visual stimuli. *Journal of the Marine Biological Association of the United Kingdom* 69(3):647-654.
7. Dill LM (1974) The escape response of the zebra danio (Brachydanio rerio) I. The stimulus for escape. *Animal Behaviour* 22(3):711-722.
8. Faulk CK, Fuiman LA, & Thomas P (1999) Parental exposure to ortho, para-dichlorodiphenyltrichloroethane impairs survival skills of Atlantic croaker (*Micropogonias undulatus*) larvae. *Environmental toxicology and chemistry* 18(2):254-262.
9. Hein AM, Gil MA, Twomey CR, Couzin ID, & Levin SA (2018) Conserved behavioral circuits govern high-speed decision-making in wild fish shoals. *Proceedings of the National Academy of Sciences* 115(48):12224-12228.
10. Paglianti A & Domenici P (2006) The effect of size on the timing of visually mediated escape behaviour in staghorn sculpin *Leptocottus armatus*. *Journal of Fish Biology* 68(4):1177-1191.
11. Kahane-Rapport SR & Goldbogen JA (2018) Allometric scaling of morphology and engulfment capacity in rorqual whales. *Journal of Morphology*:1-13.

12. Horodysky AZ, Brill RW, Crawford KC, Seagroves ES, & Johnson AK (2013) Comparative visual ecophysiology of mid-Atlantic temperate reef fishes. *Biology open* 2(12):1371-1381.
13. Horodysky AZ, Brill RW, Warrant EJ, Musick JA, & Latour RJ (2008) Comparative visual function in five sciaenid fishes inhabiting Chesapeake Bay. *Journal of Experimental Biology* 211(22):3601-3612.
14. Hedrick TL (2008) Software techniques for two-and three-dimensional kinematic measurements of biological and biomimetic systems. *Bioinspiration & biomimetics* 3(3):034001.
15. Domenici P & Blake R (1997) The kinematics and performance of fish fast-start swimming. *Journal of Experimental Biology* 200(8):1165-1178.
16. Webb PW (1984) Body form, locomotion and foraging in aquatic vertebrates. *American zoologist* 24(1):107-120.
17. Temizer I, Donovan JC, Baier H, & Semmelhack JL (2015) A visual pathway for looming-evoked escape in larval zebrafish. *Current Biology* 25(14):1823-1834.
18. Hatsopoulos N, Gabbiani F, & Laurent G (1995) Elementary computation of object approach by a wide-field visual neuron. *Science* 270(5238):1000-1003.
19. Preuss T, Osei-Bonsu PE, Weiss SA, Wang C, & Faber DS (2006) Neural representation of object approach in a decision-making motor circuit. *Journal of Neuroscience* 26(13):3454-3464.
20. Domenici P (2001) The scaling of locomotor performance in predator–prey encounters: from fish to killer whales. *Comparative Biochemistry and Physiology Part A: Molecular & Integrative Physiology* 131(1):169-182.
21. Bainbridge R (1960) Speed and stamina in three fish. *Journal of Experimental Biology* 37(1):129-153.
22. Ward AJ, Herbert-Read JE, Sumpter DJ, & Krause J (2011) Fast and accurate decisions through collective vigilance in fish shoals. *Proceedings of the National Academy of Sciences* 108(6):2312-2315.
23. Marras S, Batty RS, & Domenici P (2012) Information transfer and antipredator maneuvers in schooling herring. *Adaptive Behavior* 20(1):44-56.
24. Sharpe FA (2001) Social foraging of the Southeast Alaskan humpback whale, *Megaptera Novaeangliae*. Ph.D. Dissertation (Simon Fraser University, Burnaby, B.C.).
25. Domenici P, Blagburn JM, & Bacon JP (2011) Animal escapology I: theoretical issues and emerging trends in escape trajectories. *Journal of Experimental Biology* 214(15):2463-2473.
26. Domenici P & Batty RS (1997) Escape behaviour of solitary herring (Clupea harengus) and comparisons with schooling individuals. *Marine Biology* 128(1):29-38.
27. Domenici P & Batty RS (1994) Escape manoeuvres of schooling Clupea harengus. *Journal of Fish Biology* 45(sA):97-110.
28. Franco-Moreno R-A*, et al.* (2015) Variability and sexual dimorphism in skull morphometry of California Sea Lions (Zalophus californianus) in Mexico. *Mammalian Biology* 80(4):316-327.
29. Godfrey SJ (1985) Additional observations of subaqueous locomotion in the California Sea Lion (*Zalophus californianus*). *Aqu. Mamm* 11:53-57.

30. Feldkamp SD (1987) Swimming in the California sea lion: morphometrics, drag and energetics. *Journal of Experimental Biology* 131(1):117-135.
31. Potvin J, Cade DE, Werth AJ, Shadwick RE, & Goldbogen JA (*in review*) Gigantism and the Energetics of Lunge-Feeding Baleen Whales. *Relevant portion available pre-publication at the Stanford digital repository: https://purl.stanford.edu/mt574ws5287*.
32. Webb PW (1971) The swimming energetics of trout: II. Oxygen consumption and swimming efficiency. *Journal of Experimental Biology* 55(2):521-540.
33. Webb PW (1975) Hydrodynamics and energetics of fish propulsion. *Bulletin of the fisheries research board of Canada* 190:1-159.
34. Blake RW (1983) *Fish locomotion* (CUP Archive).
35. Fish FE (1993) Power output and propulsive efficiency of swimming bottlenose dolphins (Tursiops truncatus). *Journal of Experimental Biology* 185(1):179-193.
36. Fish FE (1998) Comparative kinematics and hydrodynamics of odontocete cetaceans: morphological and ecological correlates with swimming performance. *Journal of Experimental Biology* 201(20):2867-2877.
37. Goldbogen JA*, et al.* (2011) Mechanics, hydrodynamics and energetics of blue whale lunge feeding: efficiency dependence on krill density. *The Journal of Experimental Biology* 214(1):131-146.
38. Hemmingsen AM (1960) Energy metabolism as related to body size and respiratory surface, and its evolution. *Reports of the Steno Memorial Hospital (Copenhagen)* 13:1-110.
39. Pyenson ND (2017) The Ecological Rise of Whales Chronicled by the Fossil Record. *Current Biology* 27(11):R558-R564.
40. Rodríguez-Romero J, Palacios-Salgado D, López-Martínez J, Hernández Vázquez S, & Velázquez-Abunader J (2009) The length–weight relationship parameters of demersal fish species off the western coast of Baja California Sur, Mexico. *Journal of Applied Ichthyology* 25(1):114-116.
41. Pitcher T & Partridge B (1979) Fish school density and volume. *Marine Biology* 54(4):383-394.
42. Domenici P, Batty RS, & Similä T (2000) Spacing of wild schooling herring while encircled by killer whales. *Journal of Fish Biology* 57(3):831-836.
43. Tirelli V*, et al.* (2006) Energy density of anchovy Engraulis encrasicolus L. in the Adriatic Sea. *Journal of Fish Biology* 68(3):982-989.
44. Dubreuil J & Petitgas P (2009) Energy density of anchovy *Engraulis encrasicolus* in the Bay of Biscay. *Journal of Fish Biology* 74(3):521-534.
45. Goldbogen JA*, et al.* (2008) Foraging behavior of humpback whales: kinematic and respiratory patterns suggest a high cost for a lunge. *Journal of Experimental Biology* 211(23):3712-3719.
46. Ydesen KS*, et al.* (2014) What a jerk: prey engulfment revealed by high-rate, super-cranial accelerometry on a harbour seal (*Phoca vitulina*). *Journal of Experimental Biology* 217(13):2239-2243.
47. Chenoweth EM (2018) *Bioenergetic and economic impacts of humpback whale depredation at salmon hatchery release sites* (University of Alaska Fairbanks).